Available online at www.sciencedirect.com
ScienceDirect
Ceramics International 34 (2008) 409–416
CERAMICS INTERNATIONAL
www.elsevier.com/locate/ceramint

Effect of precursor characteristics on zirconia and ceria particle morphology in spray pyrolysis

C.Y. Chen [a,*], T.K. Tseng [b], S.C. Tsai [c], C.K. Lin [a], H.M. Lin [d]

[a] Department of Materials Science and Engineering, Feng Chia University, Taichung 407, Taiwan, ROC
[b] Department of Materials Science and Engineering, University of Florida, Gainesville, FL 32611, USA
[c] Department of Chemical Engineering, California State University, Long Beach, CA, USA
[d] Department of Materials Engineering, Tatung University, Taipei 104, Taiwan, ROC

Received 15 May 2006; received in revised form 20 July 2006; accepted 30 October 2006
Available online 13 December 2006

Abstract

Ultrasonic spray pyrolysis of acetate-based precursors with precisely measured precursor drop size was employed to produce ZrO_2 and CeO_2 particles. A bimodal size distribution of the product particles indicates a significant influence of the gas-to-particle conversion mechanism in addition to the conventionally accepted one-particle-per-drop mechanism. Due to the differences in solubility of the precursors, ZrO_2 particles are spherical in shape and smooth on their surfaces while the CeO_2 particles are bowl-like in shape with uneven surfaces. Spherical and monodispersed particles with a peak diameter <100 nm can be obtained by reducing the precursor concentrations to 0.01 wt.% in both the different precursor system.

Keywords: A. Powders: Chemical preparation; A. Precursors: organic; D. CeO_2; D. ZrO_2; Spray pyrolysis; Microstructure

1. Introduction

Spray pyrolysis has been widely used to produce fine powders because it is an inexpensive and continuous, ambient pressure process. This process is more economical than other processes (such as sol–gel and chemical vapor deposition) that involve multiple steps or that must be carried out under vacuum. Furthermore, spray pyrolysis offers numerous possibilities for controlled synthesis of advanced ceramic powders and films because of its chemical flexibility [1,2]. For example, yttria-stabilized zirconia (YSZ) has been the most commonly used solid electrolyte in solid oxide fuel cells due to its oxygen conductivity at the classical operating temperature (1000 °C) and its desirable chemical stability in both reducing and oxidizing atmospheres [3,4]. Addition of ceria to YSZ further increases the oxygen conductivity and reduces the operating temperature [5,6]. In addition, cerium oxide (ceria, CeO_2) has generated considerable interest because of its applications in gas sensors [7], catalytic supports in automotive exhaust system [8–10] and electrolyte in solid-oxide fuel cell [4,11]. Such spherical fine ZrO_2 ceramic powders with a narrow size distribution are highly desirable because they result in high reactivity and high packing density and, thus, enhancing the densification of powders with uniform microstructure at low sintering temperature [3].

Precursor drops undergo three major steps during the course of spray pyrolysis: (1) drop size shrinkage due to evaporation, (2) conversion of precursor into oxides, and (3) solid particle formation. The particle formation may involve two mechanisms: intraparticle reaction (conventional one-particle-per-drop mechanism) and gas-to-particle conversion [12]. In the one-particle-per-drop mechanism, each droplet is regarded as a micro reactor and converts into one solid particle when it travels through the tubular reactor. In contrast, gas-to-particle conversion occurs when the precursor is volatile and is transported across the particle-gas interface [12,13]. The vapor of the product materials, after being formed by chemical reaction in the gas phase, may either condense on the particles or nucleate to form new particles. Zhang et al. [14] demonstrated the influence of zirconium precursor saturation

* Corresponding author. Tel.: +886 4 24517250x5313; fax: +886 4 24510014.
E-mail address: chencyi@fcu.edu.tw (C.Y. Chen).

0272-8842/$34.00
doi:10.1016/j.ceramint.2006.10.013

concentrations on zirconia particle morphology in spray pyrolysis using a conventional ultrasonic nebulizer. They established two criteria for synthesis of solid spherical particles [14,15]: (1) the initial relative solution saturation (C_0/C_s, where C_0 and C_s are precursor concentration and precursor saturation concentration, respectively) must be ~0.01 or less; (2) the precipitated salt must not undergo plastic deformation or melting during heating.

In this work, precursor drop size was measured precisely and acetate-based zirconium and cerium precursors with drastically different solubilities were employed to determine particle morphology of the resulting YSZ and CeO_2 product powders. We found that bimodal particle size distributions were produced, suggesting that both one-particle-per-drop and gas-to-particle conversion mechanisms were involved in spray pyrolysis. We also found very different particle morphology for the two precursors used. The experimental results are consistent with the aforementioned first criterion. Dense spherical particles were produced when the initial relative solution saturations were less than ~0.01. In contrast, hollow [16] or bowl-like particles were formed as in the case of precursor cerium acetate (CeA).

2. Experimental methods

2.1. Materials preparation and product characterization

The precursors used for generation of yttria-stabilized zirconia (YSZ) particles in this study were zirconium hydroxyl acetate (ZHA)/yttria acetate hydrate (YAH) in Y_2O_3/ZrO_2 molar ratios of 3/97. The chemical formula of ZHA and YAH are $Zr(OH)_{4-x}(CH_3COO)_x$ (where $x = 1.36$, Aldrich Chem. Co., Inc.) and $(CH_3CO_2)_3Y{\cdot}xH_2O$ (Aldrich Chem. Co., Inc.), respectively, and the chemicals are reagent grade with >99% purity. Cerium acetate (CeA) was used as the precursor for production of CeO_2 particles. The chemical formula of CeA is $Ce(C_2H_3O_2)_3{\cdot}1.5H_2O$ (99.9%, Alfa Aesar, A Johnson Matthey Co.). The respective molecular weights of ZHA, YAH, and CeA reported by the manufacturers are 216, 266, and 344. The concentration of precursor solutions, YAH/ZHA and CeA in deionized water, ranged from 0.01 to 1.0 wt%. While the solubility of CeA in water is taken from the manufacturer's MSDS data, the solubility of ZHA in water is experimentally measured by heating the ZHA solution in a constant temperature bath until the ZHA precipitates, and then weighing the remaining solution. The solubility was subsequently calculated.

Characterization of the as-received precursors was carried out by thermogravimetric analysis (TGA, Perkin-Elmer Model TGA-7) under gaseous nitrogen flow for removal of product gases. The heating rate was set at 40 °C/min. The phase identification of product particles was performed by X-ray diffractometry (Philips X'pert PW3040, Philips Co., Netherlands) with Cu Kα radiation. In order to confirm the lattice structure of the doped ZrO_2, pure silicon powder was used as a standard in the XRD measurement. Moreover, the phase identification of hydrolyzed CeA was carried out on the powder precipitated from the CeA aqueous solution at approximately 80 °C. The morphology of spray pyrolyzed particles was examined using field emission scanning electron microscopy (SEM, Model 1530, Leo, Germany). Finally, the particle size distribution was determined by number counting over 500 particles from the SEM micrographs.

2.2. Spray pyrolysis system

A schematic diagram of the bench-scale spray pyrolysis system is shown in Fig. 1. Major components of the system are: (1) a three-zone furnace 130 cm in length (Linberg Model Blue M), (2) a 3 in. tubular quartz reactor (7.6 cm in i.d. and 170 cm in length) located in the furnace, (3) a conventional ultrasonic nebulizer with a resonant frequency of 1.65 MHz (King Ultrasonics Co., Ltd., Taipei, Taiwan) for generation of sprays (precursor drops), and (4) precision flow meters and controllers (MKS Model 1179, Andover, MA). As shown in this figure, the upward airflow of 20 L/min first carries the atomized precursor

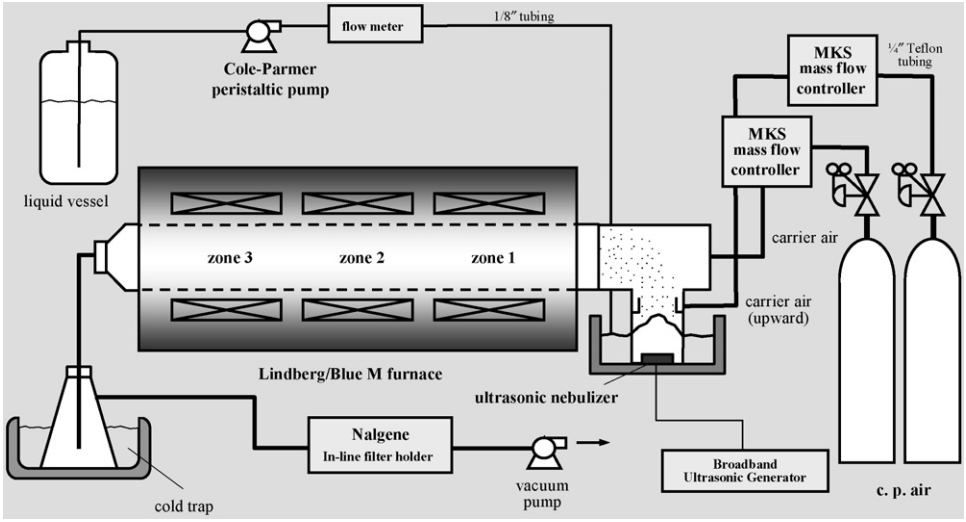

Fig. 1. Schematic diagram of spray pyrolysis system of conventional ultrasonic nebulizer.

drops into the T-adaptor where additional air at 11 L/min is provided through a distributor to carry the drops into the three-zone reactor. Thus, the total flow rate of the carrier air maintains at 31 L/min. The consumed precursor solution is ~3 cm^3/min. Provided with a vacuum pump downstream from the reactor, the carrier air controls the residence time of the precursor drops flowing through the reactor. At the maximum reactor temperature of 650 and 750 °C, the residence times of particles in the hot zones (>550 °C) are 3.2 and 4.5 s, respectively. Taking into account the expansion of the air at high temperature, calculation of the Reynold's number (790) led to the verification of laminar flow condition. The resulting product particles are collected in the cold traps and on the filter positioned between the cold traps and the vacuum pump. The temperature set point at zone 2 of the furnace is the maximum reaction temperature and the temperatures of zones 1 and 3 are set at 200 and 350 °C, respectively. The reaction temperatures used in this study were 750 °C for ZrO_2 formation and 650 °C for CeO_2 formation, respectively, since the effect of maximum reaction temperature ranging between 650 and 750 °C was found to have a negligible effect on particle size and morphology [17].

2.3. Drop size analysis

The drop sizes and size distribution were measured using the Malvern Spraytec RTS 5000. This instrument uses a solid-state laser light at 670 nm wavelength to illuminate the drops and the signal analysis is based on diffraction theory. The scattered light is collected from the forward direction by log-scaled annular detector lens that is composed of discrete elements. Because large drops scatter light at small forward angles, and small drops scatter light at large forward angles, the scattered light intensities collected by the discrete annular elements of the detector lens provide the information on drop sizes and drop size distributions that are presented as frequency plots of number percentage versus drop diameter. The instrument was calibrated using a reticle, Malvern/INSITEC Model #RS-3 and 0.5 μm-diameter particles standard. Furthermore, NIST-Traceable Microspheres with diameter ranging from 20 to 900 nm (3000 Series—Polymer Nanosphere™, Duke Scientific Corp.) were also used. All the refractive indices reported by manufacturer of the standards were set following the instruction for the instrument. The densities of the precursor drops are assumed to be 1 g/cm^3 due to the extremely dilute precursor concentrations used. Using the assumed density, the volume percentage of drop size distribution can be converted into number percentage for the comparisons with the resulting particle size distribution obtained by number counting in SEM micrographic analysis.

3. Results and discussion

3.1. Characterization of precursors and products

The TGA weight losses of the precursors used in the present study are shown in Fig. 2. Curve (a) shows that ZHA exhibits four

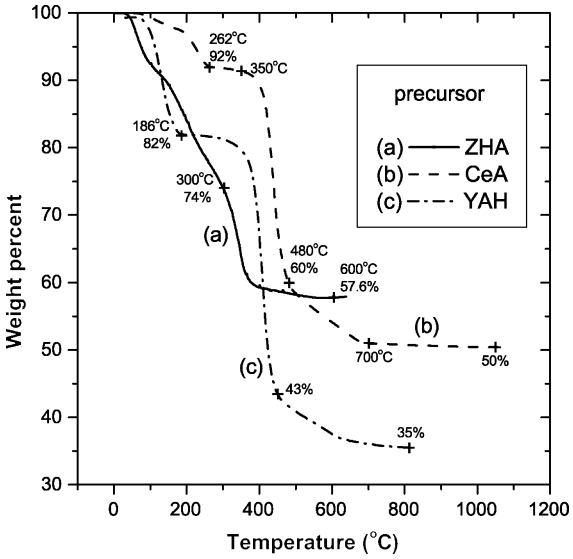

Fig. 2. Thermogravimetric analysis (TGA) curves of precursors (a) ZHA, (b) CeA, and (c) YAH.

different weight loss mechanisms in the temperature ranges of 50–150 °C, 150–300 °C, 300–400 °C, and 400–600 °C, respectively. Based on the molecular weights of ZHA and its decomposition products, the weight losses during the temperature ranges of 50–150 °C and 400–600 °C can be attributed to water evaporation and conversion into ZrO_2, respectively. The middle weight loss mechanism may be attributed to conversion of ZHA to zirconium hydroxide. Likewise, curve (b) in Fig. 2 shows that CeA experiences three major weight loss mechanisms in the temperature ranges of 200–300 °C, 350–500 °C, and 500–700 °C. The first and the last loss mechanisms are attributable to dehydration and conversion into CeO_2, respectively. The loss mechanism for the temperature range of 350–500 °C is attributed to decomposition of CeA to acetic acid and cerium hydroxide. Furthermore, the XRD data shown in the inset of Fig. 3 for the precipitates from the hydrolysis of CeA at 80 °C serve to confirm formation of cerium hydroxide. The weight loss of YAH during

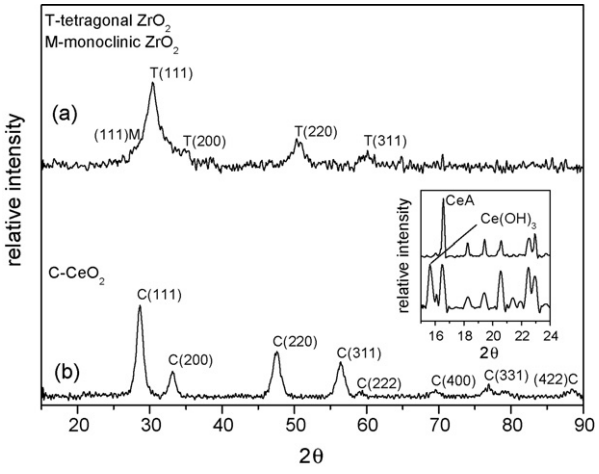

Fig. 3. The XRD patterns of particles obtained from spray pyrolyzed (a) ZHA/YAH and (b) CeA precursors. The insert shows the XRD patterns of as-received CeA and the precipitates from the hydrolysis of CeA at 80 °C.

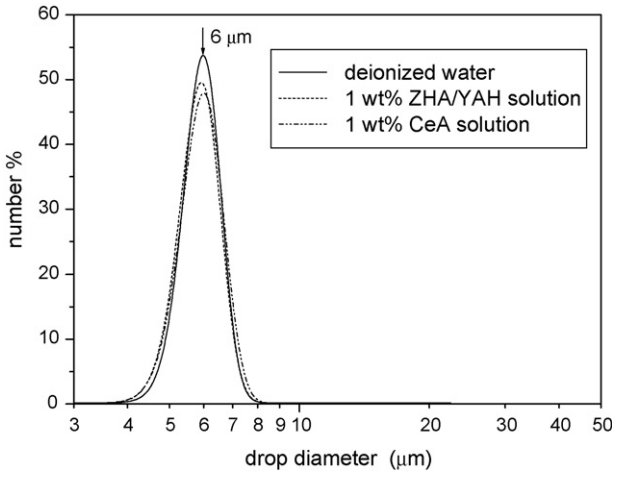

Fig. 4. The size distributions of precursor drops produced by nebulizer at 1.65 MHz.

the temperature range of 50–200 °C is attributed to the water evaporation and/or dehydration. The weight loss mechanisms are believed to result from conversion of yttrium acetate first to its hydroxide in the temperature range of 300–500 °C and subsequently from hydroxide to oxide in the temperature range of 500–750 °C.

The XRD patterns of the particles obtained from spray pyrolysis of ZHA/YAH at 750 °C and CeA at 650 °C are shown in Fig. 3, curves (a and b), respectively. Comparisons of these patterns to the standards [18,19] lead to identification of the particles obtained from ZHA/YAH precursor as YSZ and those obtained from CeA precursor as CeO_2. The dominant YSZ phase produced in this study is tetragonal structure with a small amount of monoclinic phase [20].

3.2. Comparison of particle morphologies

Fig. 4 shows the size distributions of precursor drops generated by an ultrasonic nebulizer at 1.65 MHz. It reveals

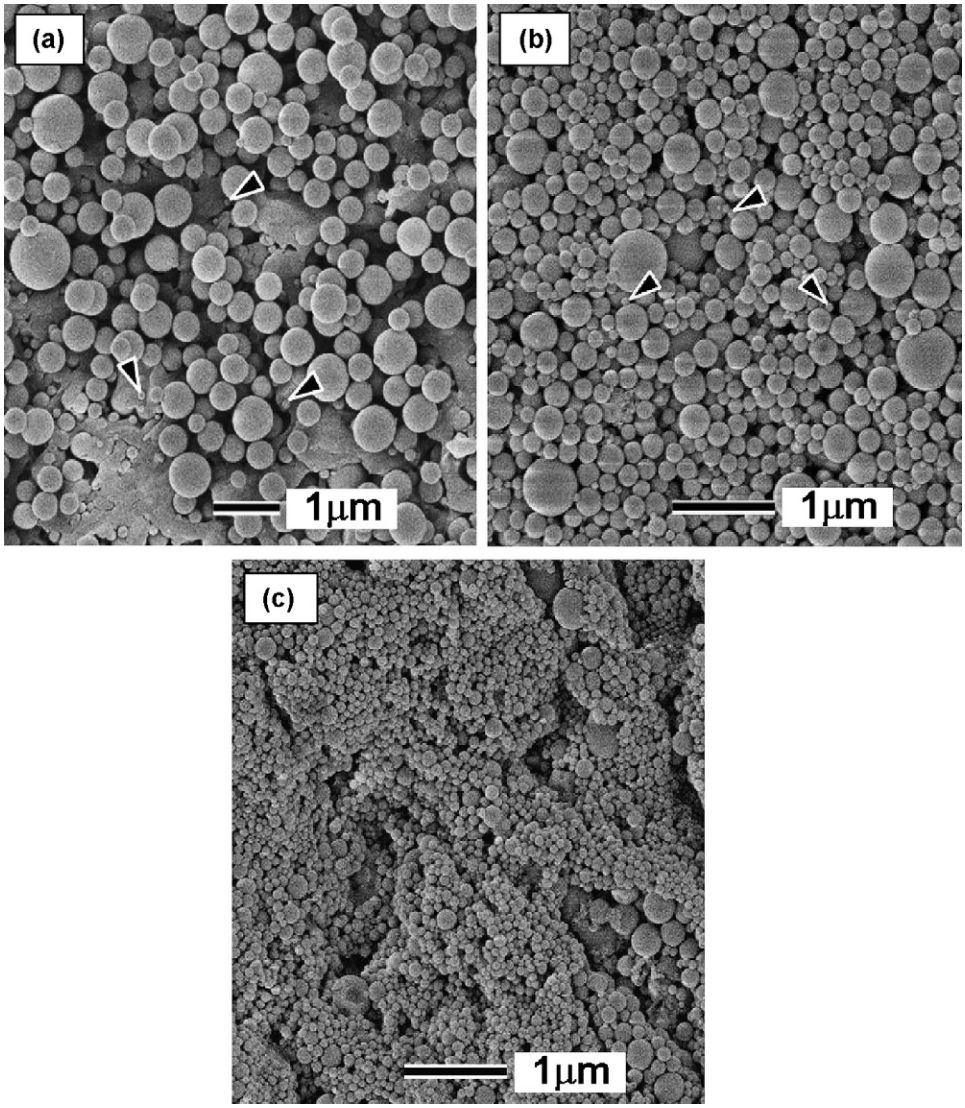

Fig. 5. SEM micrographs of YSZ particles reacted from precursor concentration of (a) 1 wt%, (b) 0.1 wt%, and (c) 0.01 wt% at reaction temperature of 750 °C. The ZHA/YAH precursor drops are produced by a nebulizer at 1.65 MHz. The small particles in (a and b) are indicated by arrows.

that the drop size distributions of both precursor solutions are almost the same as that of deionized water because the concentrations of precursors are only 1.0 wt% or lower. The drop diameters range from 4 to 8 μm with a peak diameter of 6 μm.

In earlier studies of spray pyrolysis with uniform-size drops [17,21], the product particle sizes were found to vary significantly with precursor concentrations. Therefore, three precursor concentrations (1.0, 0.1, and 0.01 wt%) were used in this study. Fig. 5 shows the SEM micrographs of the YSZ particles produced at reaction temperature of 750 °C while Fig. 6 shows those of the CeO_2 particles obtained at reaction temperature of 650 °C. For the precursor concentration ranging from 1.0 to 0.1 wt%, the YSZ particles in Fig. 5(a and b) are spherical, unagglomerated, and have smooth surfaces. In contrast, the larger CeO_2 particles in Fig. 6(a and b) for the same precursor concentration range are bowl-like with uneven surfaces. Even at precursor concentrations as low as 0.01 wt%, the majority of the larger CeO_2 particles are still uneven on surface as shown in Fig. 6(c). Note that the YSZ particles obtained at such a low precursor concentration are spherical and smooth on surface as shown in Fig. 5(c). The difference in particle morphology can be attributed to the drastic difference in precursor solubility.

The solubility of CeA precursor was found to be ~260 g/L at room temperature. In fact, when heated to 80 °C, an initially clear solution of CeA hydrolyzed and formed precipitates that were identified as cerium hydroxide by XRD as mentioned previously. Thus, the relative solution saturations at precursor concentrations of 1.0 and 0.1 wt% are greater than the critical value of 0.01 [14]. Therefore, the solute precipitates and a solid shell forms on the surface of the drop. When the solute CeA undergoes the low temperature hydrolysis, a large amount of water still exists within each drop. With increasing temperature, water vaporizes through the permeable shell of precipitated acetate or hydroxide to form hollow particles. Subsequently, plastic deformation occurs and the particles shrink and shrivel during the cooling process, resulting in uneven surfaces as shown in Fig. 6(a and b). This phenomenon was less severe in the particles generated from a precursor concentration as low as

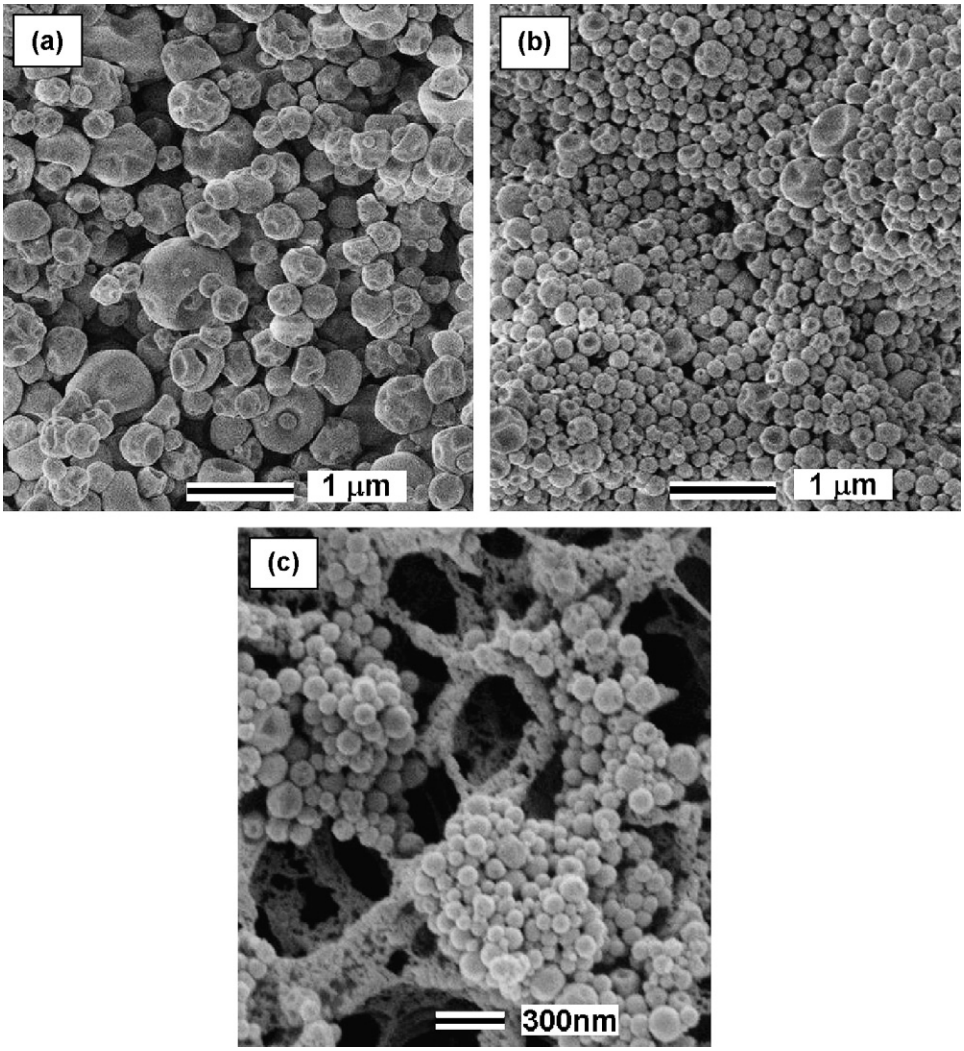

Fig. 6. SEM micrographs of CeO_2 particles reacted from precursor concentration of (a) 1 wt%, (b) 0.1 wt%, and (c) 0.01 wt% at reaction temperature of 650 °C. The CeA precursor drops are produced by a nebulizer at 1.65 MHz.

0.01 wt%. The relative solution saturation at such a dilute concentration is lower than the critical value of 0.01. As shown in Fig. 6(c), a large portion of the particles, particularly those smaller than 95 nm in diameter, are spherical and smooth on surface.

In contrast, the hydrolysis temperature of ZHA is much higher than the evaporation temperature of water, and the solubility of ZHA at room temperature is one order of magnitude higher (~8000 g/L versus ~260 g/L) than that of CeA. The relative solution saturations for ZHA concentrations of 1.0, 0.1 and 0.01 wt% are 5.2×10^{-3}, 5.1×10^{-4}, and 5.1×10^{-5}, respectively. They are significantly lower than 0.01. Consistent with the conclusions by Zhang et al. [14], volume precipitation of ZHA took place as the precursor concentration reached its saturated solubility, resulting in the ZrO_2 particles spherical in shape and smooth on surface at all studied precursor concentrations ranging from 1.0 to 0.01 wt% as shown in Fig. 5(a–c).

3.3. Comparison of particle size distributions

In the one-particle-per-drop mechanism of spray pyrolysis, each droplet is regarded as a micro reactor. It converts into solid particle when traveling through the three-zone tubular reactor. First, the diameter of the precursor drop decreases as the water solvent evaporates, resulting in an increase in precursor concentration. After the precursor drop is completely dehydrated, the precursor solute precipitates and conversion into oxide takes place without phase transformation, resulting in a dense spherical solid particle. Based on conservation of oxide mass, namely ZrO_2 in a particle = ZrO_2 in a drop, we derived the following equation for calculation of the particle diameter (d_p) from the precursor drop diameter (d) [1,14,17]:

$$d_p = d \cdot \sqrt[3]{\frac{\rho_s w}{\rho_p}} \quad (1)$$

where w is the precursor concentration in terms of weight fraction of oxide. For example, the concentration of 1 wt% ZHA converts into ZrO_2 with a weight loss of 43 wt%, $w = 0.01 \times (1 - 0.43)$, ρ_s and ρ_p are the densities of the precursor solution (1 g/cm^3) and the resulting oxide (6 g/cm^3 for ZrO_2, 7.65 g/cm^3 for CeO_2), respectively. It should be noted that this simple equation gives rise to same particle diameters as the more complex equation for the one-particle-per-drop mechanism, which takes into account the relative solution saturation [14]. Based on Eq. (1), the particle diameters for the precursor drop diameters ranging from 4 to 8 μm and precursor concentrations of 1.0, 0.1, and 0.01 wt% were calculated. The results are listed in Table 1. This table shows that in spite of same precursor drop diameter, the product CeO_2 particles are significantly smaller than the product YSZ particles due to the greater density of the former.

The predicted particle diameters are also shown in Fig. 7: solid curve for precursor ZHA/YAH and dotted curve for precursor CeA. Note that the peak drop diameter of 6 μm. is identical to the mean drop diameter because of the symmetrical drop size distributions as shown in Fig. 4. Both the experimental data (open circles and open squares) and the theoretical curves in Fig. 7 show decreased particle diameter with decreasing precursor concentration. However, the experimentally measured particle diameters are clearly smaller than the particle diameters predicted by the Eq. (1) one-particle-per drop mechanism.

Table 1
The particle size predicted by the one-particle-per-drop mechanism

Precursor drop size (μm)	ZHA/YAH concentration (wt%)			CeA concentration (wt%)		
	1.0	0.1	0.01	1.0	0.1	0.01
	Predicted product particle size (nm)					
4	393	182	84	347	161	74
5	492	228	105	434	201	93
6 (peak)	590	274	127	520	242	112
7	688	319	148	607	282	131
8	786	365	169	694	322	150
Measured mean particle size	354	162	84	351	185	94

The precursor solution concentrations involved are 1.0, 0.1 and 0.01 wt%, respectively. The measured mean sizes are also listed.

The particle diameters measured by SEM micrographic analysis represent over-estimated particle diameters for bowl-like CeO_2 particles that are uneven on surface because they are assumed to be spherical in our estimation. More than 500 particles were thus counted to obtain the mean CeO_2 particle diameters represented by the open squares in Fig. 7. Nevertheless, these mean particle diameters are significantly smaller than the predicted values for 6 μm mean drop diameter. This may indicate that vaporization of precursor CeA during heating takes place to a significant degree and some CeO_2 particles are formed via the gas-to-particle conversion mechanism rather than the one-particle-per-drop mechanism. The evaporation of the CeA leads to smaller oxide particles. Moreover, the oxide vapor, after being formed

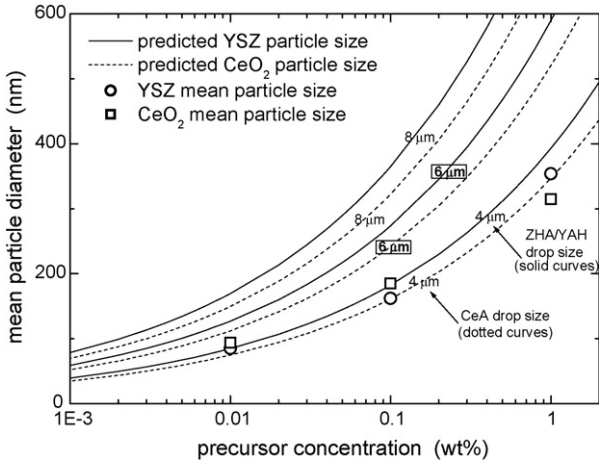

Fig. 7. Mean particle size diameter of resulting particles as a function of precursor concentration. The drop size (6 μm) enclosed in small box is the peak drop diameter. The theoretically predicted particle sizes from various drop diameters are also shown as a function of precursor concentration.

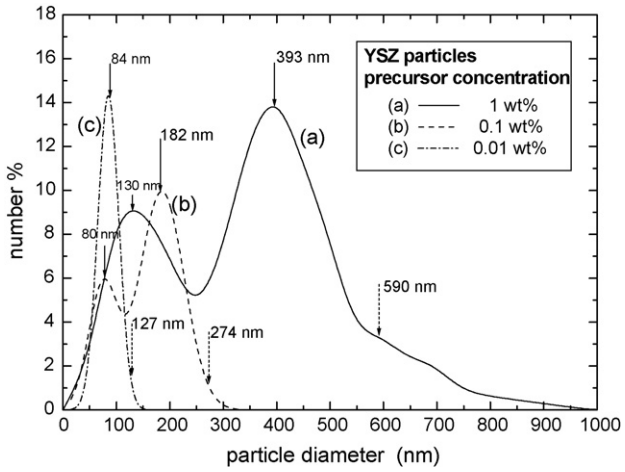

Fig. 8. Size distributions of YSZ particles obtained from ZHA/YAH precursor concentrations of (a) 1 wt%, (b) 0.1 wt%, and (c) 0.01 wt% at reaction temperature of 750 °C. Particle diameters next to dotted arrows are calculated by Eq. (1) for drop diameter of 6 μm.

by chemical reaction of the precursor in the gas phase, may nucleate to form new small particles.

Curves (a–c) in Fig. 8 depict the YSZ particle size distributions obtained from spray pyrolysis of ZHA/YAH at 750 °C and respective precursor concentrations of 1.0, 0.1, and 0.01 wt%. Curves (a and b) clearly show bimodal distributions. The larger peak particle diameters (393 and 182 nm) are significantly smaller than those (590 and 274 nm) predicted for the peak (or mean) drop diameter of 6 μm. The corresponding smaller peak diameters (130 and 80 nm) are also found to be considerably smaller.

Fig. 9 shows the CeO_2 particle size distributions obtained from CeA precursor concentrations of (a) 1.0 wt%, (b) 0.1 wt%, and (c) 0.01 wt% after being pyrolyzed at 650 °C. Like the YSZ particles, curve (a) shows a broad particle size distribution with two peaks at 340 and 100 nm. The larger peak particle diameter (340 nm) of the CeO_2 particles is close to that

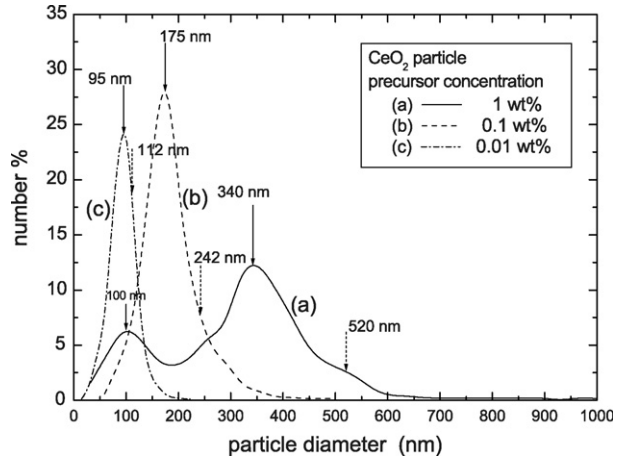

Fig. 9. Size distributions of CeO_2 particles obtained from CeA precursor concentrations of (a) 1 wt%, (b) 0.1 wt%, and (c) 0.01 wt% at reaction temperature of 650 °C. Particle diameters next to dotted arrows are calculated by Eq. (1) for drop diameter of 6 μm.

predicted by the one-particle-per-drop mechanism for the smaller drops (4 μm in diameter) at 1.0 wt% precursor concentration, but significantly smaller than that (520 nm) predicted for the 6 μm mean drop diameter. In contrast, curves (b and c) show single peak diameters at 175 and 95 nm for precursor concentrations of 0.1 and 0.01 wt%, respectively. These peak diameters are larger than the corresponding CeO_2 particle diameters (161 and 74 nm) for 4 μm drop diameter, but smaller than those (242 and 112 nm) for the peak drop diameter of 6 μm predicted by the one-particle-per-drop mechanism (see Table 1). The cumulative number percentages of particles smaller than those predicted for 4 μm drop diameter at precursor concentrations of 1.0, 0.1, and 0.01 wt% are approximately 66, 62, and 53% for YSZ particles, respectively. The corresponding cumulative number percentages for CeO_2 particles are 65, 59, and 30%.

The bimodal particle size distributions observed can be attributed to two different mechanisms: one-particle-per-drop mechanism for the larger peak diameter particles and gas-to-particle conversion mechanism for the smaller peak diameter particles. The gas-to-particle conversion occurs when the precursor is volatile, resulting in the formation of new particles from the vaporized precursor species [12]. As a result, ultra fine particles can be found in the micrographs of Fig. 5(a and b) and Fig. 6(a). Fig. 8 also shows that the difference between the larger and the smaller peak particle diameters decreases as the precursor concentration is reduced from 1.0 to 0.1 wt%. A further decrease in precursor concentration to 0.01 wt% results in a very narrow particle size distribution with a single peak at 84 nm as shown in Fig. 8 curve (c) for YSZ particles. Likewise, a narrow size distribution with a single peak at 95 nm is seen in Fig. 9 curve (c) for CeO_2 particles.

4. Conclusion

The solubility of precursors in spray pyrolysis is shown to significantly influence the morphology of the product particles. The large solubility of ZHA/YAH renders the product YSZ particles being spherical, unagglomerated, and smooth on surfaces. In contrast, the low solubility of CeA results in CeO_2 particles being bowl-like in shape with uneven surfaces. By precise measurement of the precursor drop size, we show that the gas-to-particle conversion mechanism is also involved in spray pyrolysis, and thus resulting in particle sizes much smaller than those predicted by the one-particle-per-drop mechanism alone.

Acknowledgement

This research was partially sponsored by the National Science Council, the Republic of China, under the Grant No. NSC93-2216-E-035-026.

References

[1] G.L. Messing, S.C. Zhang, G.V. Jayanthi, Ceramic powder synthesis by spray pyrolysis, J. Am. Ceram. Soc. 76 (11) (1993) 2707–2726.

[2] L. Vergnieres, P. Odier, F. Weiss, C.-E. Bruzek, J.-M. Saugrain, Epitaxial thick films by spray pyrolysis for coated conductors, J. Eur. Ceram. Soc. 25 (12) (2005) 2951–2954.
[3] S.T. Aruna, K.S. Rajam, Synthesis characterisation and properties of Ni/PSZ and Ni/YSZ nanocomposites, Scripta Mater. 48 (5) (2003) 507–512.
[4] N.Q. Minh, Ceramic fuel cells, J. Am. Ceram. Soc. 76 (3) (1993) 563–588.
[5] H.L. Tuller, A.S. Nowick, Doped ceria as a solid oxide electrolyte, J. Electrochem. Soc. 122 (2) (1975) 255–259.
[6] H. Yahiro, Y. Baba, K. Eguchi, H. Arai, High-temperature fuel cell with ceria-yttria solid electrolyte, J. Electrochem. Soc. 135 (8) (1988) 2077–2080.
[7] H.-J. Beie, A. Gnörich, Oxygen gas sensors based on CeO_2 thick and thin films, Sens. Actuators B 4 (1991) 393–399.
[8] M. Ogita, K. Higo, Y. Nakanishi, Y. Hatanaka, Ga_2O_3 thin film for oxygen sensor at high temperature, Appl. Surf. Sci. 175–176 (2001) 721–725.
[9] H. Xu, L. Gao, H. Gu, J. Guo, D. Yan, Synthesis of solid, spherical CeO_2 particles prepared by the spray hydrolysis reaction method, J. Am. Ceram. Soc. 85 (1) (2002) 139–144.
[10] T.C. Rojas, M. Ocaña, Uniform nanoparticles of Pr(III)/ceria solid solutions prepared by homogeneous precipitation, Scripta Mater. 46 (9) (2002) 655–660.
[11] R.N. Blumentthal, F.S. Brugner, J.E. Garnier, The electrical conductivity of CaO-doped nonstoichiometric cerium oxide from 700 °C to 1500 °C, J. Electrochem. Soc. 120 (9) (1973) 1230–1237.
[12] T.T. Kodas, M.J. Hampden-Smith, Aerosol Processing of Materials, Wiley-Vch, New York, 1999, p. 421.
[13] A.S. Gurav, T.T. Kodas, J. Joutsensaari, E.I. Kauppinen, R. Zilliacus, Gas-phase particle size distributions and lead loss during spray pyrolysis of (Bi, Pb)–Sr–Ca–Cu–O, J. Mater. Res. 10 (7) (1995) 1644–1652.
[14] S.-C. Zhang, G.L. Messing, M. Borden, Synthesis of solid, spherical zirconia particles by spray pyrolysis, J. Am. Ceram. Soc. 73 (1) (1990) 61–67.
[15] G.V. Jayanthi, S.C. Zhang, G.L. Messing, Modeling of solid particle formation during solution aerosol thermolysis—the evaporation stage, Aerosol Sci. Technol. 19 (4) (1993) 478–490.
[16] S. Jain, D.J. Skamser, T.T. Kodas, Morphology of single-component particles produced by spray pyrolysis, Aerosol Sci. Technol. 27 (5) (1997) 575–590.
[17] Y.L. Song, S.C. Tsai, C.Y. Chen, T.K. Tseng, C.S. Tsai, J.W. Chen, Y.D. Yao, Ultrasonic spray pyrolysis for synthesis of spherical zirconia nanoparticles, J. Am. Ceram. Soc. 87 (10) (2004) 1864–1871.
[18] Joint Committee on Powder Diffraction Standards (JCPDS) card for X-ray diffraction 26–0345.
[19] JCPDS card for X-ray diffraction 74–0665.
[20] W. Nimmo, D. Hind, N.J. Ali, E. Hampartsoumian, S.J. Milne, The production of ultrafine zirconium oxide powders by spray pyrolysis, J. Mater. Sci. 37 (16) (2002) 3381–3387.
[21] Y. Itoh, M. Abdullah, K. Okuyama, Direct preparation of nonagglomerated indium tin oxide nanoparticles using various spray pyrolysis methods, J. Mater. Res. 19 (4) (2004) 1077–1086.